Outline of climate and oceanic conditions in the Indian Ocean: an update to mid-2019

Francis MARSAC[1] & Hervé DEMARCQ[2]
IRD
UMR MARBEC, Station Ifremer
Sète, France

Abstract

The trend in climate and oceanic variables was investigated for the recent years (2017-2019). After a neutral phase in 2018, the Southern Oscillation Index entered a negative phase in January 2019, continuing until July 2019. This short event has been qualified as a weak El Niño event. By contrast, a positive dipole (IOD), started in 2017, continued through 2018 and was still observed at a lesser level in August 2019. In line with the IOD, from 2017 to present, warm temperature anomalies prevailed in the WIO whereas sea surface temperature fluctuated around the average in the EIO. The trend in chlorophyll concentration (SSC) was investigated in four ecoregions of the tropical Indian Ocean, distributed between 12°N and 30°S, during 1997-2019. A similar trend is observed in the four ecoregions, with SSC-depleted conditions during 2007-2014 and SSC-enhanced conditions in 2015-2019. A different pattern was observed from 1998 to 2006. Finally, following previous studies, it is shown that the intensity of two important upwelling systems of the tropical Indian Ocean fluctuate in relation to the Dipole/ENSO cycle, however in an opposite way. In the EIO, the SLP anomalies recorded in Darwin can have a predictive power by indicating the status of the Java-Sumatra upwelling in the 3 coming months.

1- Introduction

Several descriptors of the ocean status are examined to depict the inter-annual variability and to track trends in the large pelagic ecosystem. We investigate the inter-annual dynamics in the primary productivity of four large ecoregions of the Indian Ocean. Furthermore, we study inter-annual changes in two coastal upwelling, the Somali upwelling in the West Indian Ocean and the Java-Sumatra upwelling in the East Indian Ocean (EIO. To some extent, the environmental descriptors form a complementary set of information that can be useful to inform the WPTT for the stock management advice.

2- Data sources

Various sources of data are used in this paper:

- climate indices based on *(i)* sea level pressure anomalies, such as the Southern Oscillation Index (SOI) that depicts the ENSO cycle, and the Indian Ocean Oscillation Index (IOI, Marsac and Le Blanc, 1998); and *(ii)* a sea surface temperature-derived index, the Dipole Mode Index (DMI, Saji et al, 1999) reflecting a mode of variability that is specific to the Indian Ocean (and sometimes coupled to the ENSO).
- Sea surface chlorophyll-a (SSC) concentration from SeaWifs (1997-2002) and Modis (2003-present) satellite-mounted sensors, giving an index of ocean surface productivity (enhancement or depletion).
- sea surface temperature (SST) from the ERSSTv4 dataset (Huang et al, 2015), a monthly product at a 2° grid resolution. This dataset is used to compute the DMI.

[1] Email : francis.marsac@ird.fr
[2] Email : herve.demarcq@ird.fr

- sea surface temperature from the OISSTv2 dataset (*NOAA_OI_SST_V2 data provided by the NOAA/OAR/ESRL PSD, Boulder, Colorado, USA, https://www.esrl.noaa.gov/psd/)* available since November 1981 at a 1°grid/month resolution (Reynolds et al, 2002), used in this paper for maps and in the analysis of the two selected upwelling systems.
- NOAA/NCEP Global Ocean Data Assimilation System (GODAS) providing monthly fields of temperature, salinity, vertical velocity and current for 40 depth levels (5 to 4500 m), along a 1° longitude/0.33° latitude grid globally. Here, we use the model product to derive the depth of thermocline by interpolating the 20°C isothermal depth between consecutive temperature at depth in the upper 300m of the water column.

More details on the datasets and methods used to produce the variables can be found in Marsac (2013). All data have been updated to August 2019.

3- Variability and trends in the oceanic environment

3.1 Climate indices

The **SOI** indicates that the last El Niño event (positive phase of the ENSO cycle) occurred from March 2015 to April 2016, with peak activity observed from May 2015 to March 2016 (Fig. 1a). The conditions returned to normal and kept that status until December 2018. Strongly negative SOI values occurred in January 2019, then returned to less negative values until July 2019. Considering all variables associated to ENSO (and not displayed here) the Climate Prediction Center of the NOAA (http://cpc.ncep.noaa.gov/products/CDB) qualified this event (January to July 2019) as weak El Niño conditions.

An ensemble analysis of multiple models (18 dynamical models and 8 statistical models) predicts a 75% chance that ENSO-neutral conditions prevail during the Northern Hemisphere fall 2019, and 55-60% chance that it would continue through Spring 2020 (Fig. 2) (NOAA, 2019).

The **IOI** was dominated by negative values (reflecting low pressure anomalies and warm conditions in the West IO) over several years, from 2007 through 2015. A positive IOI developed for almost 12 months through the second semester of 2016 and first quarter of 2017. A negative IOI has developed since February 2019 and the value recorded for June, July and August 2019 were still negative (-2.2, -1.9, -1.2 respectively) (Fig. 1b)

The **DMI** went through 3 significant positive phases during the past 12 years: 2007 (coincident to an El Niño event), 2012 and 2017-2018 (and again growing since May 2019). Negative dipoles were less marked than positive dipoles, and were observed in 2005, 2010 and 2016 (Fig. 3). Several statistics were calculated from the DMI series. 16% of monthly values are associated to recognized dipole events, either positive or negative. Among the positive DMI values, 13% of them corresponded to recognized positive dipole events (above the threshold of 0.4). Among the negative DMI values, 22% denoted recognized negative dipole events. The climate perturbations occur when positive dipoles arise in coincidence with El Niño, and negative dipoles with La Niña. The IOD+/Niño combination may cause droughts in the Eastern Indian Ocean (EIO) and severe rainfall anomalies in the Western Indian Ocean (WIO). An opposite response arises with the IOD-/ Niña combination.

An ensemble analysis of several models predicts a further development of the positive dipole through October-November 2019, followed by a gradual return to quasi-normal conditions by March 2020 (Australian Bureau of Meteorology, 2019) (Fig. 4).

We further analysed the SST anomalies in the two boxes used to compute the DMI: Wbox (40°-50°S / 10°N-10°S) in the WIO and Ebox (90°E-110°S / 0°-10°S) in the EIO. Over the period Jan-2015 through Aug-2019, the ocean remained anomalously warm in the Wbox with almost all months being above the 3rd quartile of the SST anomalies distribution for 1970-2019 (+0.25). In the Ebox, SST anomalies remained positive in 2016 (as anomalies in the Wbox were declining) and the 2017-2018 series remained in the neutral to negative domain, with 3 months crossing the 1st quartile boundary (-0.29) (Fig. 5).

All three indices are significantly correlated, with the highest correlation found between IOI and SOI (r_s = +0.46, $p<.001$). With respect to DMI, the highest correlation is found with IOI (r_s = -0.23, $p<0.001$)

compared to that with SOI (rs = -0.15, p<0.001) which makes sense as DMI and IOI include a mode of variability which is specific to the Indian Ocean.

3.2 Main oceanic features over 2017-2019

Maps of anomalies for SST, the 20°C isothermal depth and SSC are presented in Fig. 6 (a to f).

- Positive SST anomalies developed in the WIO from May to October 2017 in relation with the growing positive dipole, however the thermocline remained shallower than normal in the latitudinal band 2°S-8°S west of 90°E. The sea surface chlorophyll (SSC) remained around normal or slightly negative in the WIO. Elevated SSC levels were observed West, South and East of Indian.
- In 2018, SST anomalies fluctuated between moderately warm and cold anomalies in the WIO. Cold anomalies started to develop in the Java upwelling in May, at the onset of the south-east monsoon. Shallow thermocline in the WIO was observed until March 2018, then deep thermocline started to develop in April in the south tropical gyre, peaking in Dec 2018-Jan 2019 with a 50-60 deepening of the 20°C isothermal depth. Patches of high SSC were located between the African coast and Seychelles from May to July, whereas SSC was normal over most of the tropical IO south of 12°N.
- In 2019, warmer SST expanded northwards, from the Mascarene basin to the Arabian Sea. SSC was normal from March to May. Patches of high SSC appeared in the Java upwelling in June and were still observed in August 2019.

4- Inter-annual variability and trends of primary productivity in four ecoregions of the Indian Ocean

Four large ecoregions were defined for this analysis on the basis of the work developed at the recent Ecoregion workshop of the IOTC which was held in La Reunion (30 Aug-1 Sept 2019) prior to the WPEB15. Actually, the version of draft ecoregion used here is a simplified version of the workshop's draft proposal. We consider two ecoregions (MONW in the West, MONE in the East, separated at 77°E) within the large MONS Longhurst province (Longhurst 1998). Our MONW ecoregion also encompasses the Somalian part of the Longhurst's ARAB province. We also delineate an ecoregion for the Mozambique Channel (MOZ), basically the northern region of the Longhurst's EAFR province excluding the east coast of Madagascar. Finally the 4th ecoregion matches the almost entire Longhurst's ISSG province. The four ecoregions (Fig. 7) are defined within the following boundaries:

- MONW : 40°S - 77°E / 10°N – 12°S
- MONE : 77°E - 120°E / 10°N – 12°S (excluding regions extending east of Sumatra and north of Java)
- MOZ : 30°E – 47°S / 12°S – 30°S
- ISSG : 47°E – 120°E / 12°S – 30°S

In order to compare the overall productivity of each ecoregion, we computed the SSC annual average as displayed in Fig. 8. The MOZ region is the most productive one, MONW ranks second, MONE ranks third and the less productive region is the ISSG. However, we must keep in mind that 1997 and 2019 are incomplete years in terms of observations. SeaWifs measurements started in September 1997 and the Modis measurements were collected until August 2019.

MOZ SSC concentration ranged from 0.33 to 0.44 mg.m^{-3} with a period of higher productivity from 1998 to 2002 and a slight increase to an average of 0.40 mg.m^{-3} for 2015-2019 after 10 years of low productivity. The lowest SSC value was recorded in 1997 when a strong El Niño and positive dipole was developing. The mesoscale vertical dynamics caused by eddies propagating through the Mozambique Channel and the chlorophyll-rich waters of the Mozambican and western Madagascan shelfs, transported offshore by the action of eddies, contribute to generate an average enhanced productivity in this region.

MONW SSC concentration ranged from 0.16 to 0.24 $mg.m^{-3}$ with peaks of enhanced productivity recorded in 2004-2005 and during 2016-2018. Likewise MOZ, the lowest recorded SSC value was in 1997.

By contrast to the two previous Western IO provinces, an anomalously high SSC concentration was recorded in 1997 (0.36 $mg.m^{-3}$), when the coupled Niño/IOD+ event boosted the production in the eastern edge of the Indian Ocean. Apart from 1997, the SSC in MONE ranged from 0.15 to 0.21 $mg.m^{-3}$. High SSC values were recorded in 2006 (when a moderate Niño/IOD+ event was developing). The last three years of the series (2017-2019) have been among the most productive years since 1998.

Finally, SSC in ISSG fluctuated in a short range, between 0.09 and 0.13 $mg.m^{-3}$ denoting oligotrophic conditions. Slightly higher concentration was observed in 2000 and during the last 3 years of the series.

The series were normalized to perform a direct comparison of inter-annual changes across ecoregions. The normalization consists in calculating the deviation (in %) of each year to the multi-annual mean, in each region. The normalized series (Fig. 9) exhibit interesting features:

- The two western ecoregions (MONW and MOZ) were negatively affected by the 1997 coupled Niño/IOD+ event with 20% and 12% reduction in SSC concentration, respectively; whereas a twofold increase of SSC occurred in the eastern region (MONE). By contrast, the 1997 coupled Niño/IOD+ event did not cause any particular signal in ISSG;
- In ISSG and western ecoregions, a phase with positive SSC anomalies prevailed from 1998 to 2006, but with a time shift across ecoregions. The first "anomalous wave" of SSC enhancement concerned ISSG (+17.2% in 2000), then MOZ (+15.2% in 2002) and finally MONW (+18.9% in 2004). This SSC-enhanced phase had a different time span across the ecoregions: 4 years in ISSG, 5 years in MOZ, 6 years in MONW.
- During the above described positive phase, the SSC showed an opposite situation in MONE. When SSC was back to normal in the ISSG, MOZ and MONW, strong positive SSC anomalies were measured in MONE, coincident to the development of a Niño/IOD+ event.
- From 2007 on, all four ecoregions followed the same overall pattern, dominated by a low productivity from 2007 to 2014 (reaching a maximum of -20% reduction), and a shift to positive productivity (up to 10% increase) from 2015 to 2019.

Such changes in trends between ecoregions before and after 2007 deserve further investigation. With only 23 years at hand, the current series is too short to elaborate on possible cycle in the productivity of the Indian Ocean based on satellite observations. Analyses based on biogeochemical models simulations are required.

5- Inter-annual changes in two major coastal upwelling systems

In the WIO, the northern summer bloom along the Somali is associated with upwelled waters deflecting off the coast at two locations, forming two cold wedges at around 2°-4°N and 8°-9°N and creating a two-gyre system (Brown et al, 1980; Schott, 1983) known as the Great Whirl and the Southern Gyre. The result is an offshore export of primary production in the western part of the MONW ecoregion. Another source of chlorophyll enhancement in that ecoregion is the curl-driven upwelling (also known as the Seychelles-Chagos thermocline ridge) reaching its maximum during the southwest monsoon. Here we focus on the Somali upwelling.

In the EIO, an upwelling develops during the Southeast monsoon (June to October) along the coast of Java and Sumatra as a response to regional winds. The upwelling terminated at the onset of northwest monsoon.

5.1 Somali upwelling

The months of July to September, corresponding to the peak of the southwest monsoon, were selected to track changes in the monthly SST over an area extending 500 km offshore from the Somali coastline (Fig. 10a), during 1982-2019. SST fluctuated at inter-annual scale from 24.7°C to 26°4°C (Fig. 10b). Several of the major SST anomalies coincide with large deviations of the mean July-September IOI (Fig. 10c). In 1983 and 1987, known as El Niño events, the IOI was largely negative and the upwelling was weaker (higher SST). SST also tended to be above normal in 2007, during another coupled El Niño-

IOD+ event. On the opposite, the upwelling was more intense in 1986, 1996 and 2016 during positive IOI episodes. However, several years did not show this pattern, such as 1994 with low SST and negative IOI, and 2009 with high SST and positive IOI. We used a GAM to investigate the relationship. The July-September average of the IOI is highly significant and the GAM explains 42.7% of the deviance.

```
SSTSom_JAS ~ s(IOI_JAS, bs = "cs")

Parametric coefficients:
            Estimate Std. Error t value Pr(>|t|)
(Intercept) 25.57102    0.04884   523.5   <2e-16 ***
---

Approximate significance of smooth terms:
            edf  Ref.df     F   p-value
s(IOI_JAS)  4.525  9    2.471   0.00136 **
---

R-sq.(adj) =  0.347   Deviance explained = 42.7%
GCV = 0.10608  Scale est. = 0.090658  n = 38
```

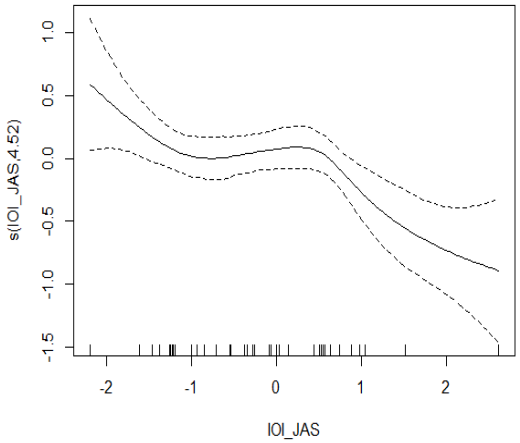

The SSC response during July-September generally fluctuates in an opposite way to the SST (Fig. 10d). We investigated whether IOI could also explain the SSC fluctuations. The GAMs results (below) show that positive IOIs are associated with higher Chlorophyll concentration in the Somali region. This simple model, almost linear, explains almost 31% of the deviance.

```
LnChl_JAS ~ s(IOI_JJA, bs = "cs")

Parametric coefficients:
            Estimate Std. Error t value Pr(>|t|)
(Intercept) -0.57213    0.01377  -41.55   <2e-16 ***
---

Approximate significance of smooth terms:
             edf    Ref.df     F     p-value
s(IOI_JJA)   1.431    9      0.924   0.011 *
---

R-sq.(adj) =  0.261   Deviance explained = 30.9%
GCV = 0.0048774  Scale est. = 0.0043619  n = 23
```

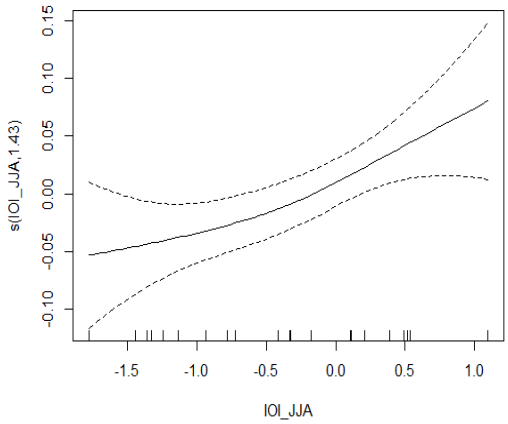

5.2 Java-Sumatra upwelling

We selected SST for July-September, at the peak of the southeast monsoon, in a large area extending south of Sumatra and Java where the austral winter upwelling takes place (Fig. 11a). SST during that season exhibited large fluctuations, from 22.5 to 28.5°C from 1982 to 2019 (Fig 11b). One major cause of climatic variability in the Indo-Pacific is the Southern Oscillation, and the nearest location from the study area which indicates such oscillation is Darwin (North Australia) where the Sea Level Pressure anomalies (SLPa) are used to calculate the SOI. A combined time series plot shows opposite fluctuations between SST during July to September and Darwin SLPa in June (Fig 11c). The GAM used to study

this linkage indicates that the SLPa in June is highly significant to explain SST fluctuations during the 3 following months, as shown below :

```
SST_JAS ~ s(SLPa_Dar_Jun, bs = "cs")

Parametric coefficients:
            Estimate Std. Error t value Pr(>|t|)
(Intercept) 26.63306    0.08239   323.3   <2e-16 ***
---

Approximate significance of smooth terms:
                 edf   Ref.df   F   p-value
s(SLPa_Dar_Jun)   3.509   9    3.27  4.71e-05 ***
---

R-sq.(adj) =  0.433   Deviance explained = 48.7%
GCV = 0.29265  Scale est. = 0.25792   n = 38
```

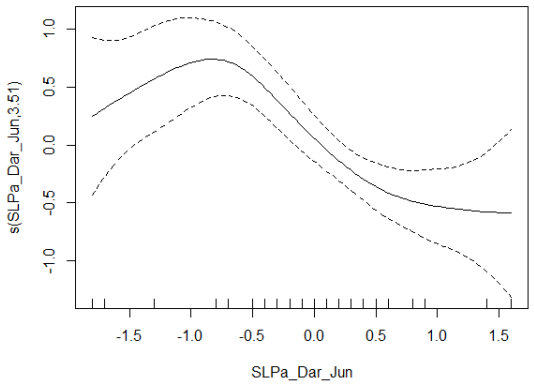

As expected, the SSC response is inversely related to the SST (Fig. 11d). It is noteworthy that the highest SSC concentration was observed during the development of the coupled Niño/IOD+ event, during the second semester of 2007. An opposite pattern was observed in the Somali upwelling. The relationship between SSC during the upwelling season (July-September) and June SLP anomalies in Darwin was investigated with a GAM (below). The SLPa is significantly related to the fluctuations of the Chlorophyll and the model explained 36.4% of the deviance.

```
LnChl_JAS ~ s(SLPa_Dar_Jun, bs = "cs")

Parametric coefficients:
            Estimate Std. Error t value Pr(>|t|)
(Intercept) -0.36612    0.03097  -11.82 2.74e-10 ***
---

Approximate significance of smooth terms:
                 edf Ref.df     F p-value
s(SLPa_Dar_Jun) 2.695      9 1.081  0.0271 *
---

R-sq.(adj) =  0.276   Deviance explained = 36.4%
GCV = 0.026283  Scale est. = 0.02206   n = 23
```

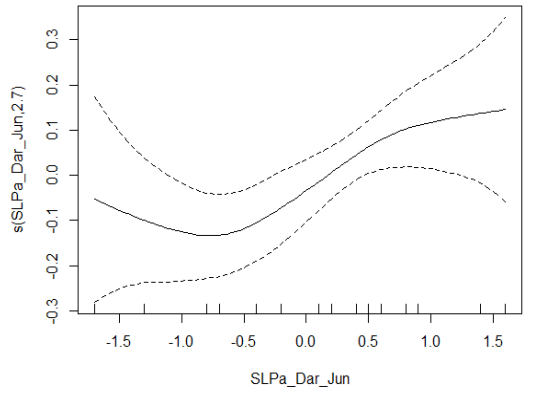

5.3 Discussion

The fluctuations observed in SST and SSC in both upwelling systems show a direct link with the inter-annual climatic variability in the Indian Ocean. The Somali upwelling tends to be weaker during warm events related to positive IO dipole, while the Java-Sumatra upwelling intensifies during El Niño events (i.e. positive dipoles).

Sea level pressure measurements, from which the IOI is derived, are variables to consider to indicate trends in the upwelling intensity. As the primary productivity generated by the upwelling is transported offshore in two anticyclonic gyres (the Great Whirl and the Southern Gyre) and sustains a trophic food

chain along the path of water mass motion, any significant decline in the upwelling can cascade into the food web and negatively affect foraging conditions for top predators. Wiggert et al (2006) indicate that both gyres exhibit a biological response, which is stronger in the Great Whirl compared to the Southern gyre. It is noteworthy that drifting objects (FOBs) are temporarily trapped into the Great Whirl, with large biomass of juvenile tuna associated to them. On the average, tunas get an advantage to reside in this area during the southwest monsoon, however it is not clear yet if changes in tuna abundance associated to FADs occur during the anomalously warm years caused by positive IODs and low IOIs.

The Java-Sumatra upwelling is also closely associated to the ENSO cycle, with lower (higher) SSC produced during La Niña (El Niño) events. Murtugudde et al. (2000) concluded that the anomalous cooling in that region was driven both locally, by strengthened, upwelling-favorable winds off Sumatra, and remotely by strengthened equatorial easterlies. Highly positive (negative) SLP anomalies in Darwin are indicative of El Niño (La Niña) events, thus the reasonable degree of deviance explained by the GAM used to explore the linkage between the upwelling SST and SLP anomalies on one hand, and between the biological response and SLP anomalies on the other hand. The interesting point is that SLP measurements in Darwin have a somewhat predictive power on the degree of SSC enrichment in the Java-Sumatra upwelling. Indonesia is the first tuna fishing country in the Indian Ocean, in terms of total catches, and such SSC fluctuations are useful to consider in monitoring and management of Indonesian fisheries.

6- Conclusion

The environmental conditions in the IO have fluctuated in relation to the Indian Ocean Dipole. The most recent event, a positive dipole, started in 2017, continued through 2018 and was still observed at a lesser level in August 2019. Further development of the positive dipole is expected through October-November 2019, followed by a gradual return to quasi-normal conditions by March 2020. Basically, 2015 was a warm year in the WIO and moderately warm in the EIO, 2016 was a warm year in the EIO whereas temperature were back to normal in the WIO during the 2nd semester. Finally, from 2017 to present, warm anomalies prevailed in the WIO and around-normal temperature in the EIO.

An analysis carried out in four large ecoregions of the Indian Ocean concluded to a similar trend from 2007 to present, although the SSC levels (and associated processes) in each region are different. The trend depicted SSC-depleted conditions during 2007-2014 and SSC-enhanced conditions in 2015-2019. The earlier period 1998-2006 was SSC-enriched in the western ecoregions, including ISSG, however the enrichment took place during different time windows of 4 to 6 years duration. Opposite conditions occurred in the EIO.

Finally, the intensity of two important upwelling systems of the tropical Indian Ocean fluctuates in relation to the Dipole/ENSO cycle, however in an opposite way. In the EIO, the SLP anomalies recorded in Darwin can indicate the status of the Java-Sumatra upwelling in the 3 coming months with some potential for fisheries monitoring and management in that region.

Acknowledgements

We are grateful to the Climate Centre of the Seychelles National Meteorological Services, and particularly to Marcel Belmont, a senior technician of this Centre, for the provision of sea level pressure data used to compute the IOI.

References

Brown, C.R., Bruce, J.G., Evans, R.H. (1980). Evolution of sea surface temperature in the Somali Basin during the southwest monsoon of 1979. *Science* 209: 595-597

Bureau of Meteorology, Australia (2019). Indian Ocean Dipole outlooks. http://www.bom.gov.au/climate/enso/#tabs=Indian-Ocean

Huang, B., Banzon, V.F. , Freeman, E. , Lawrimore, J., Liu, W., Peterson, T.C., Smith, T.M., Thorne, P.W. Woodruff, S.D. and Zhang, H.-M. (2015). Extended Reconstructed Sea Surface Temperature version 4 (ERSST.v4): Part I. Upgrades and intercomparisons. *J. Climate*, doi:10.1175/JCLI-D-14-00006.1

Longhurst, A. (1998). The ecological geography of the sea. Academic Press.

Marsac, F. (2012). Outline of climate and oceanographic conditions in the Indian Ocean over tye period 2002-2012. *14th Session of the Working Party on Tropical Tuna*. IOTC-2012-WPTT14-09, 16 p.

Marsac, F. (2013). Outline of climate and oceanographic conditions in the Indian Ocean: an update to August 2013. *15th Session of the Working Party on Tropical Tuna*. IOTC-2013-WPTT15-09, 14 p.

Marsac, F., Le Blanc, J-L. (1998). Interannual and ENSO-associated variability of the coupled ocean-atmosphere system with possible impacts on the yellowfin tuna fisheries of the Indian and Atlantic oceans. In: J.S. Beckett (Ed). *ICCAT Tuna Symposium. Coll. Vol. Sci. Pap*., L(1) : 345-377.

Murtugudde, R., McCreary, J.P., Busalacchi, A. J. (2000). Oceanic processes associated with anomalous events in the Indian Ocean with relevance to 1997–1998. *J. Geophys. Res.*, 105 : 3295–3306.

NOAA, 2019. Climate Diagnostics Bulletin August 2019. Near real-time ocean/atmosphere, monitoring, assessment and prediction. 89 p.

Reynolds, R.W., Rayner, N.A. , Smith, T.M., Stokes, D.C., and Wang, W. (2002): An improved in situ and satellite SST analysis for climate. *J. Climate*, 15, 1609-1625

Saji, N.H., Goswani, B.N., Vinayachandran, P.N., Yamagata, T. (1999). A dipole mode in the tropical Indian Ocean. *Nature* 401: 360-363

Schott, F. (1983). Monsoon response of the Somali Current and associated upwelling. *Prog. Ocean*. 12 : 357-381.

Susanto, R., Gordin, A.J., Zheng, Q. (2001). Upwelling along the coast of Java and Sumatra and its relation to ENSO. *Geophys Res. Lett.* 28(8: 1599-1602

Wiggert, J.D., Murtugudde, R.G., Christian, J.R. (2006). Annual ecosystem variability in the reopical Indian Ocean: results of a coupled bio-physical ocean general circulation model. *Deep Sea Res II*, 53: 644-676

(a)

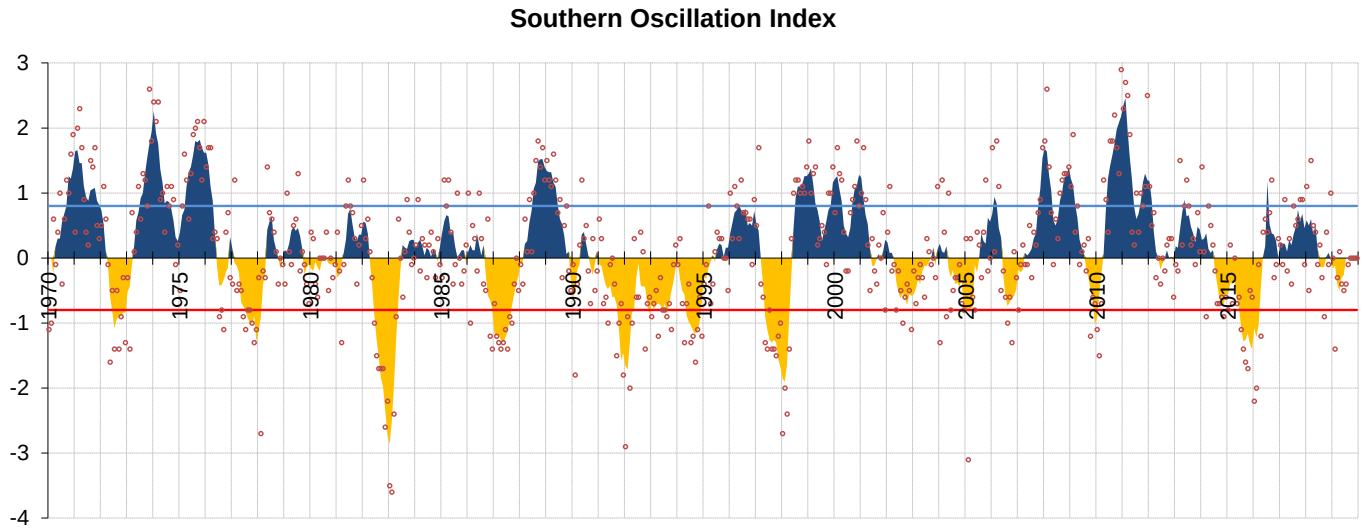

(b)

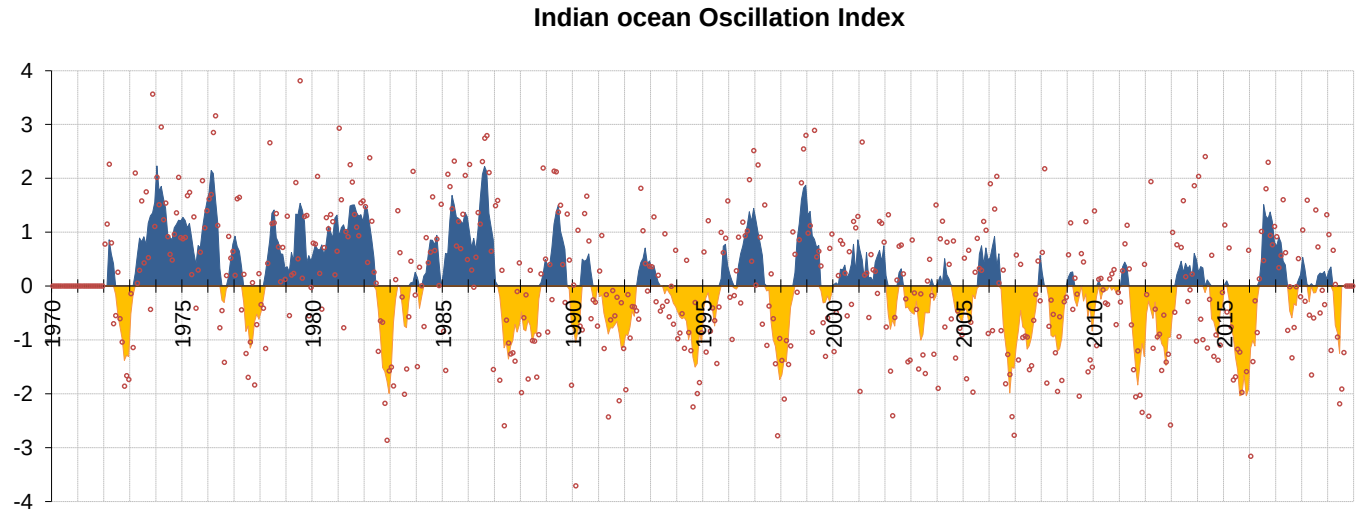

Fig.1 – (a) The Southern Oscillation Index (SOI) and (b) the Indian Oscillation Index (IOI), January 1970 to August 2019. The color shaded area represents the 5-month moving average, whereas observed monthly values are shown in red dots. El Niño events correspond to the extreme negative values whereas La Niña events are described by the extreme positive values of the SOI.

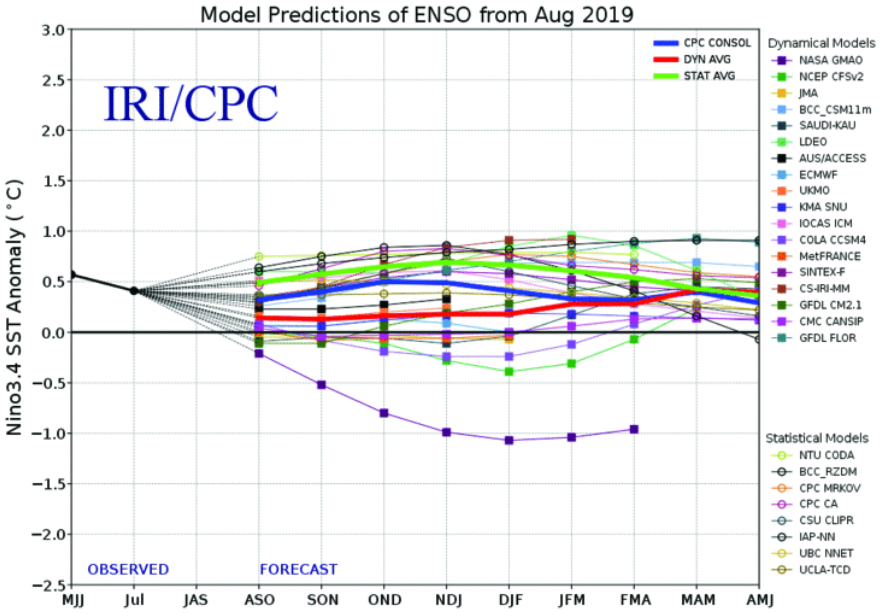

Fig.2 – SST anomalies forecast for Niño 3-4 region (East Pacific ocean) indicating the forecasted trend of the SOI from August-September-October 2019 to April-May-June 2020 (NOAA, 2019)

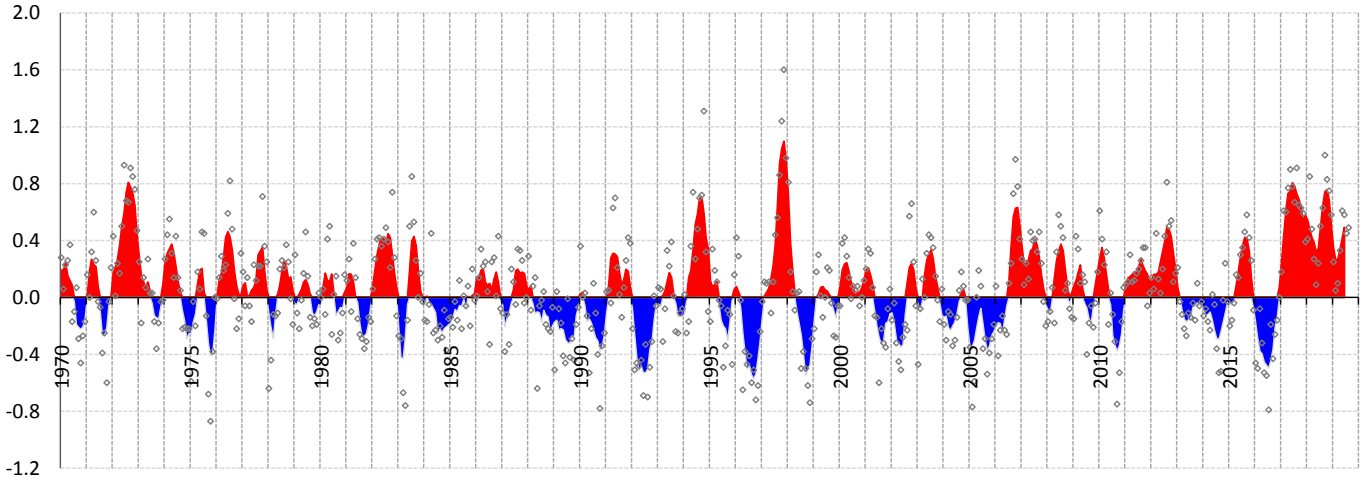

Fig.3 - Dipole mode, January 1970 – August 2019. The shaded area of IOI is a 5-months moving average whereas observed monthly values are represented in black empty dots. The DMI series is 5-month moving average. For a given anomaly, IOI and DMI are frequently in opposite sign.

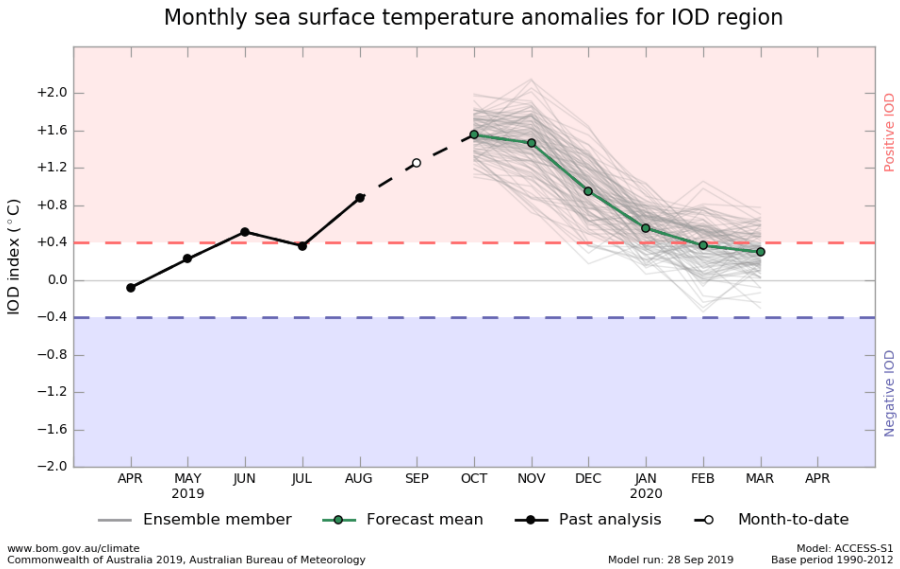

Fig.4 – Dipole mode forecast through predicted monthly sea surface anomalies for the Dipole mode region (Australian Bureau of Meteorology http://om.gov.au/climate/enso/)

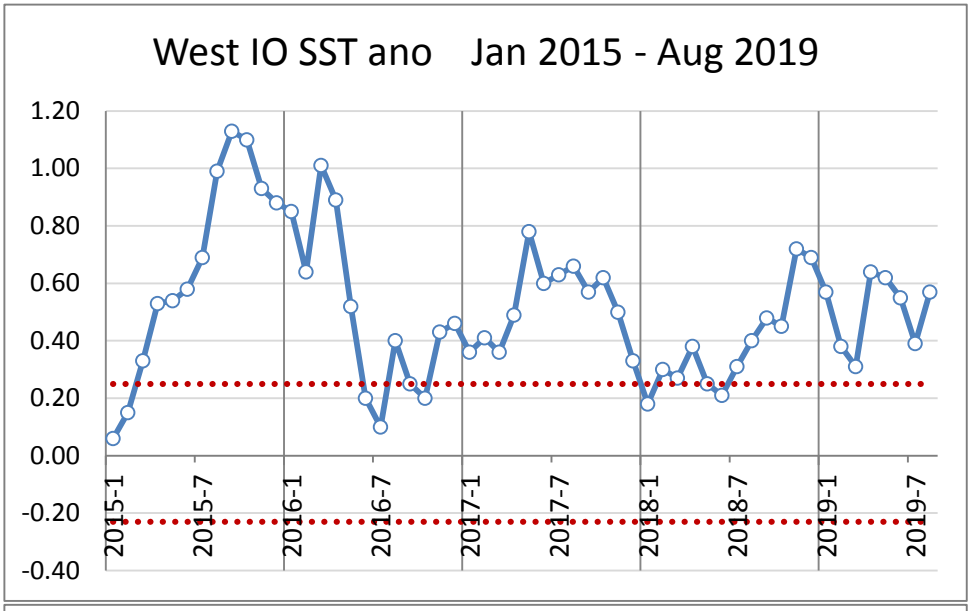

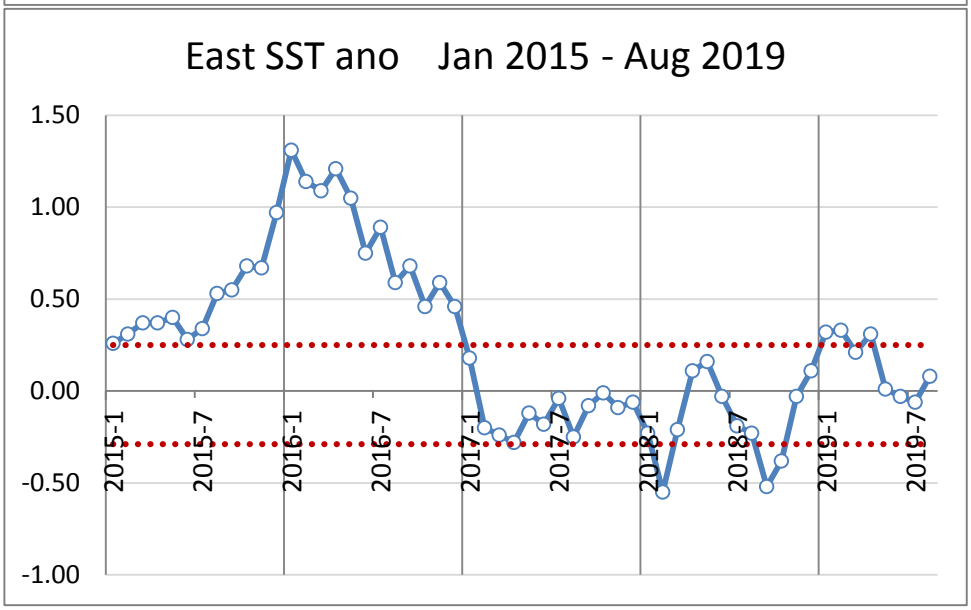

Fig.5 -Non-smoothed SST anomalies in the Western and Eastern boxes used to compute the DMI, for January 2015-August 2019.
Top: Wbox (40°E-50°S / 10°N-10°S).
Bottom: Ebox (90°S-110°S / 0°-10°S).

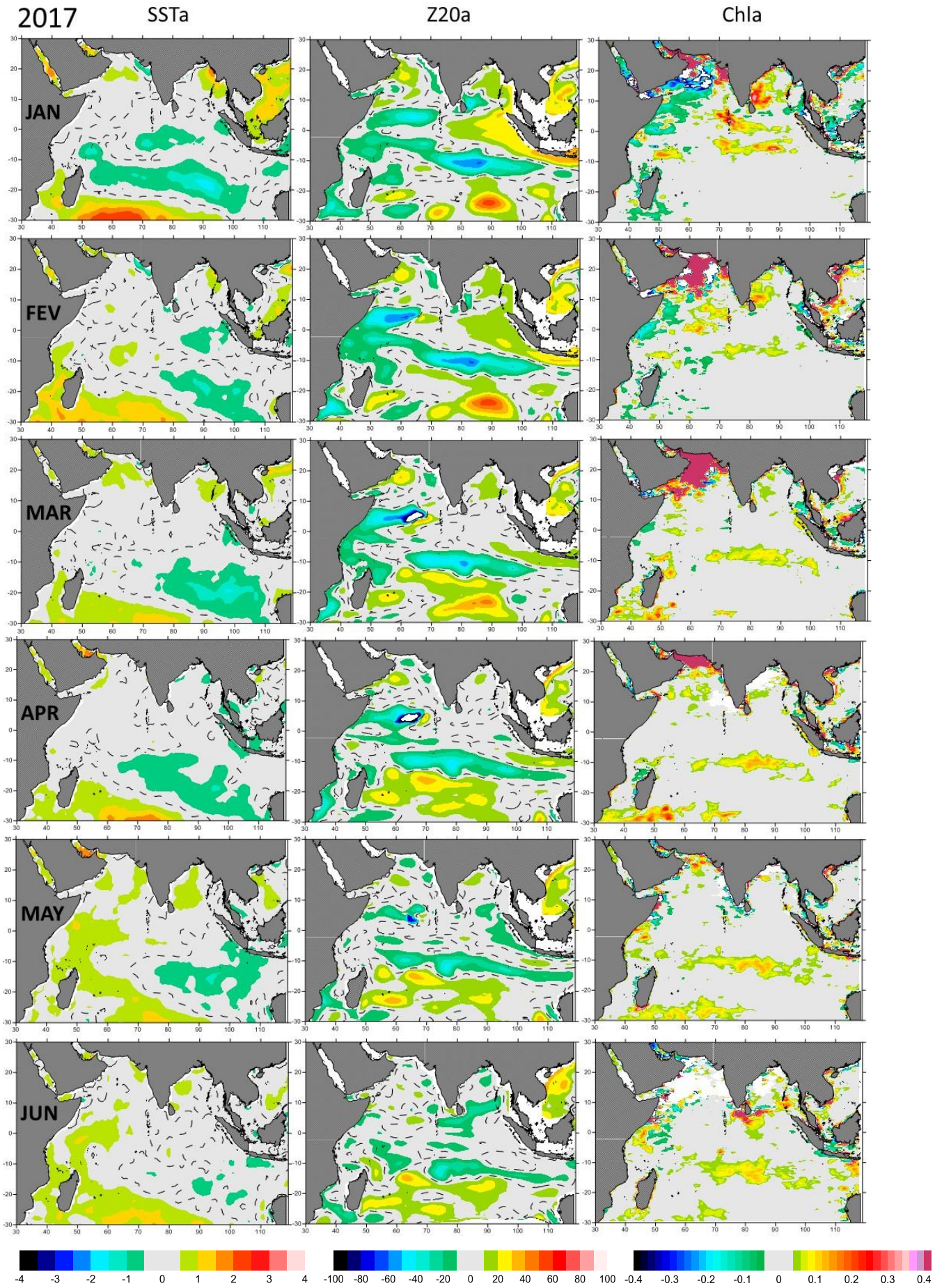

Fig. 6a – Geographic distribution of anomalies for sea surface temperature (°C, left), 20°C isothermal depth (m, middle) and sea surface chlorophyll (mg.m^{-3}, right) for the first semester of 2017. Grey shading indicates minor anomalies about the mean. Thus, the more significant anomalies (colour shading) are displayed.

.

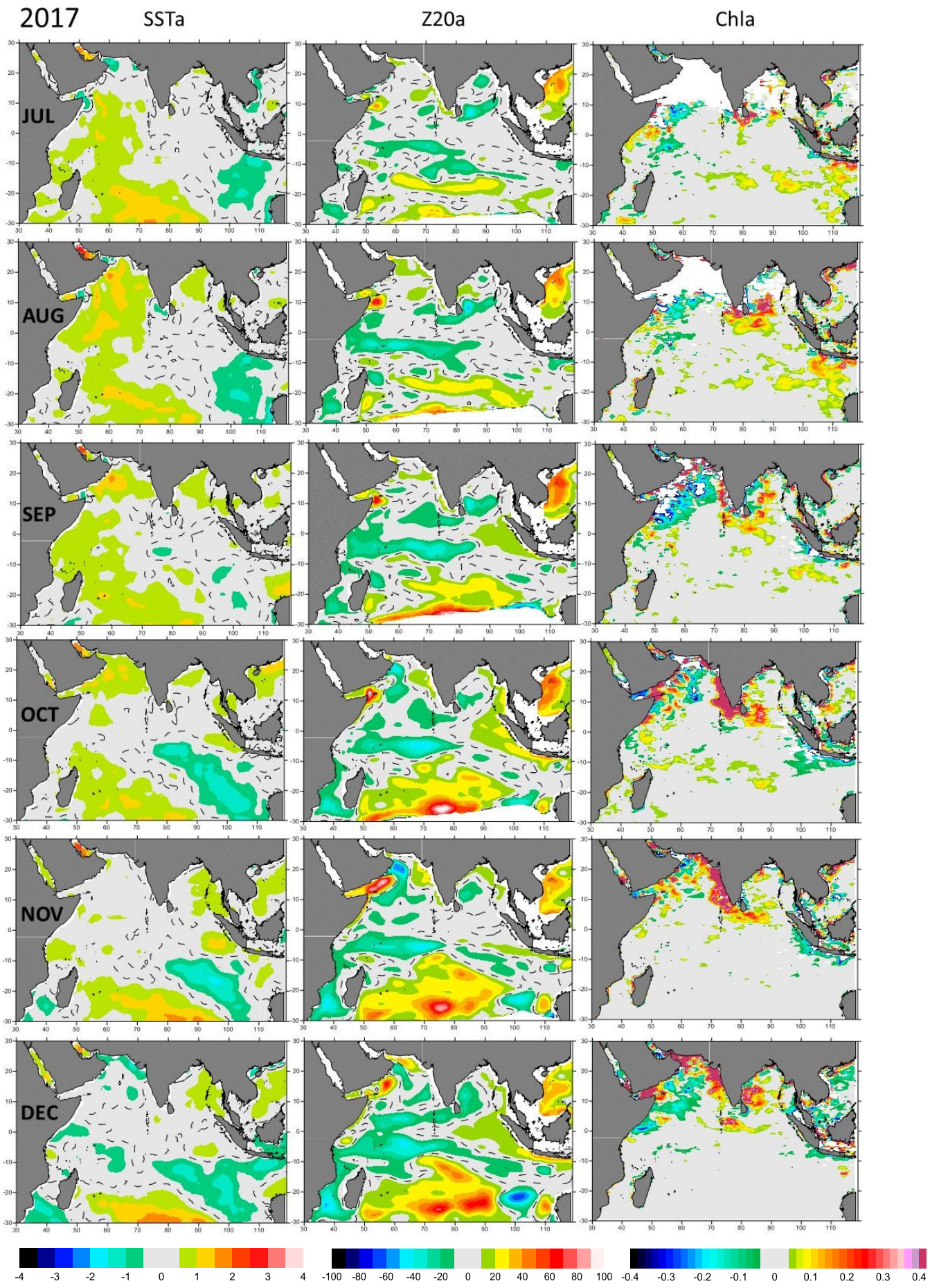

Fig. 6b – Same as above, for the second semester of 2017.

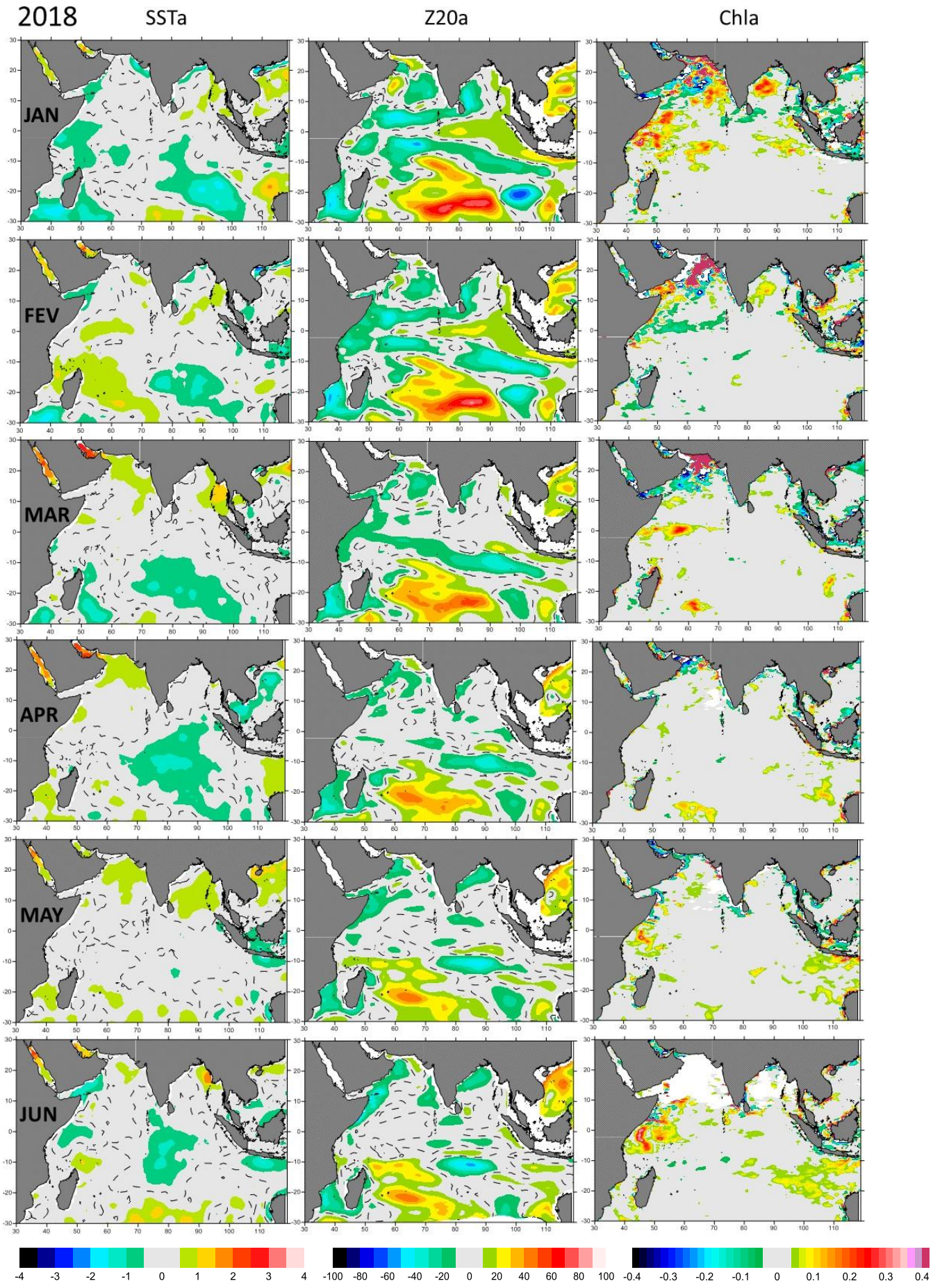

Fig. 6c – Same as above, for the first semester of 2018.

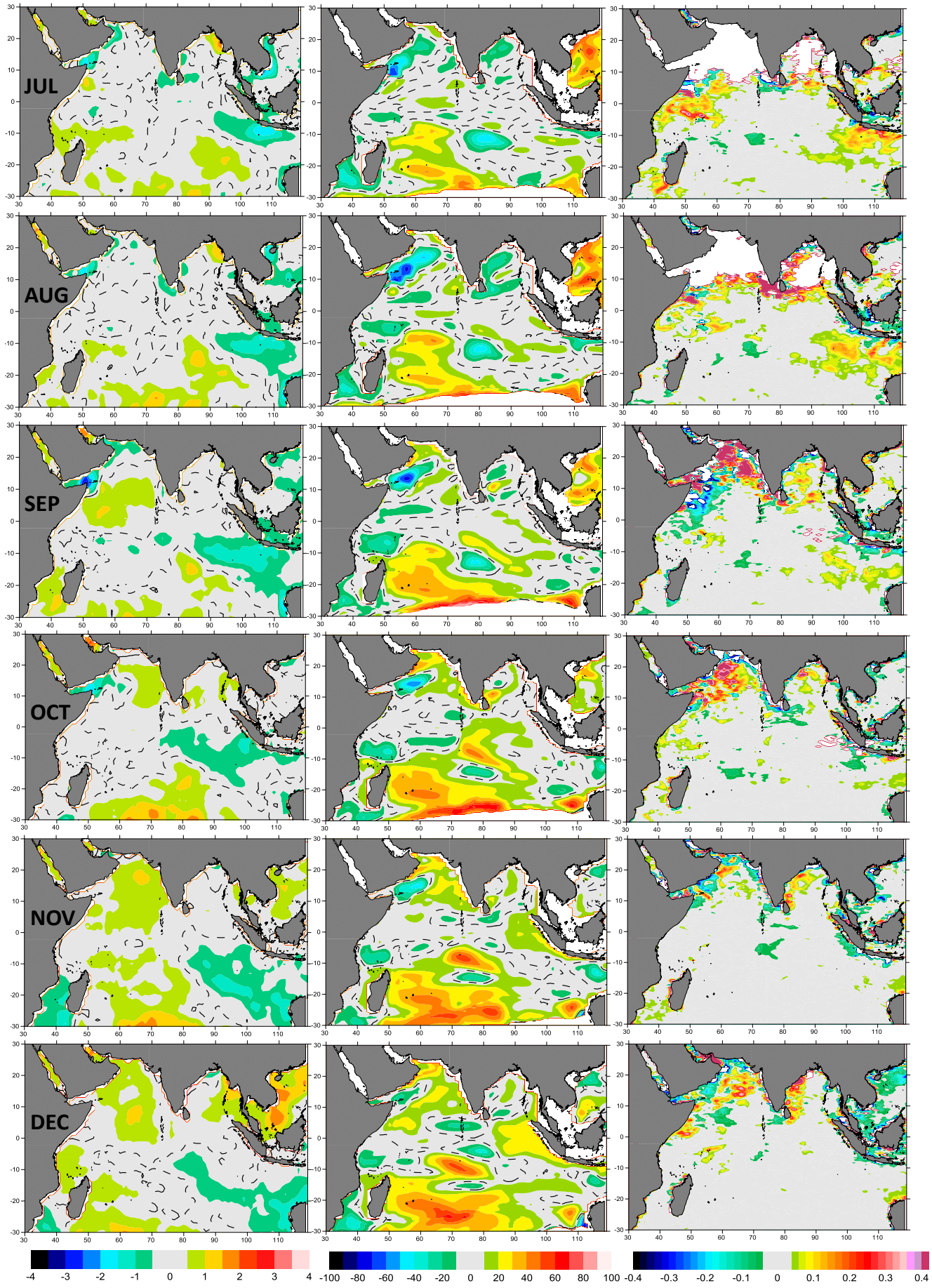

Fig. 6d – Same as above, for the second semester of 2018

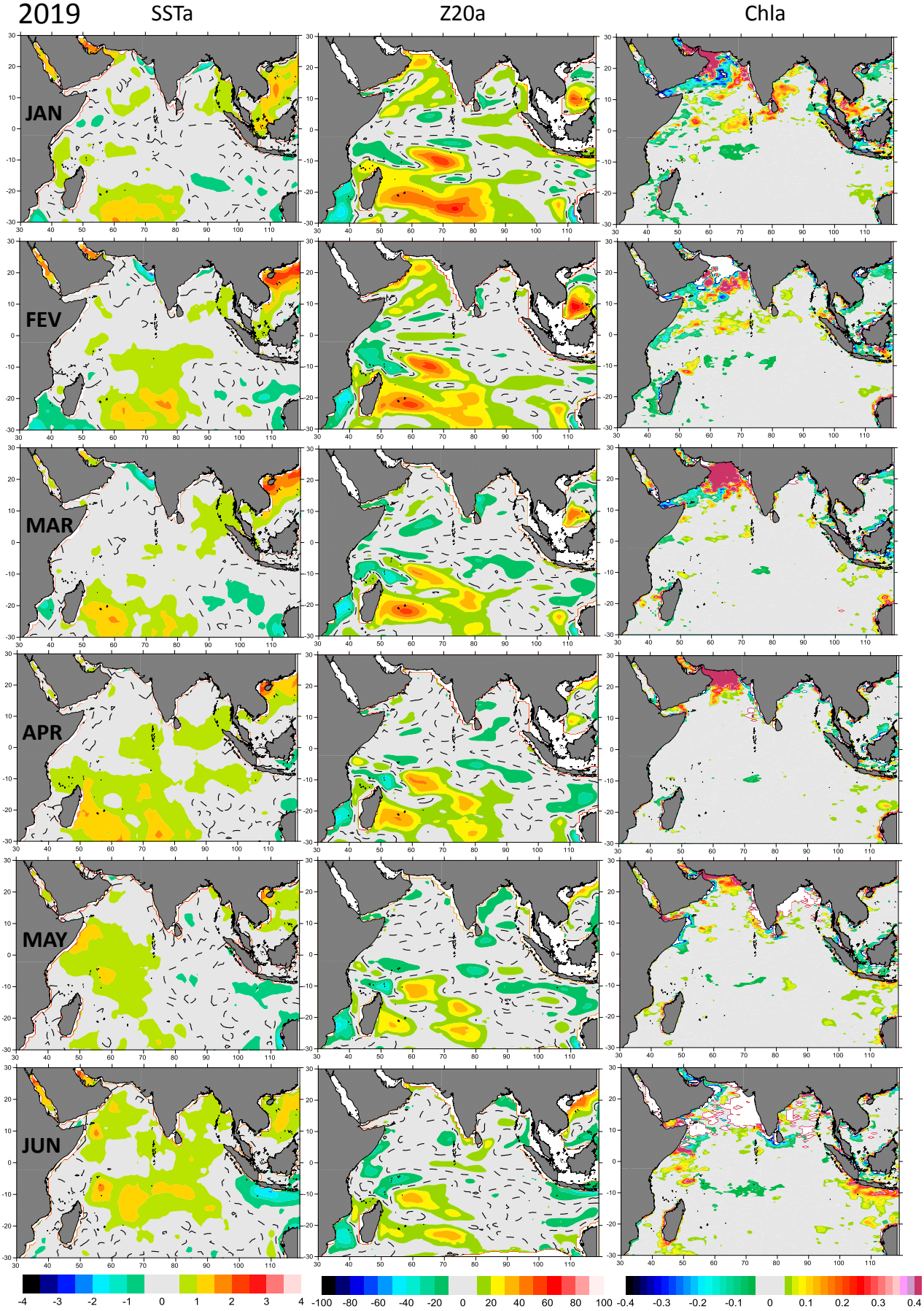

Fig. 6e – Same as above, for the first semester of 2019

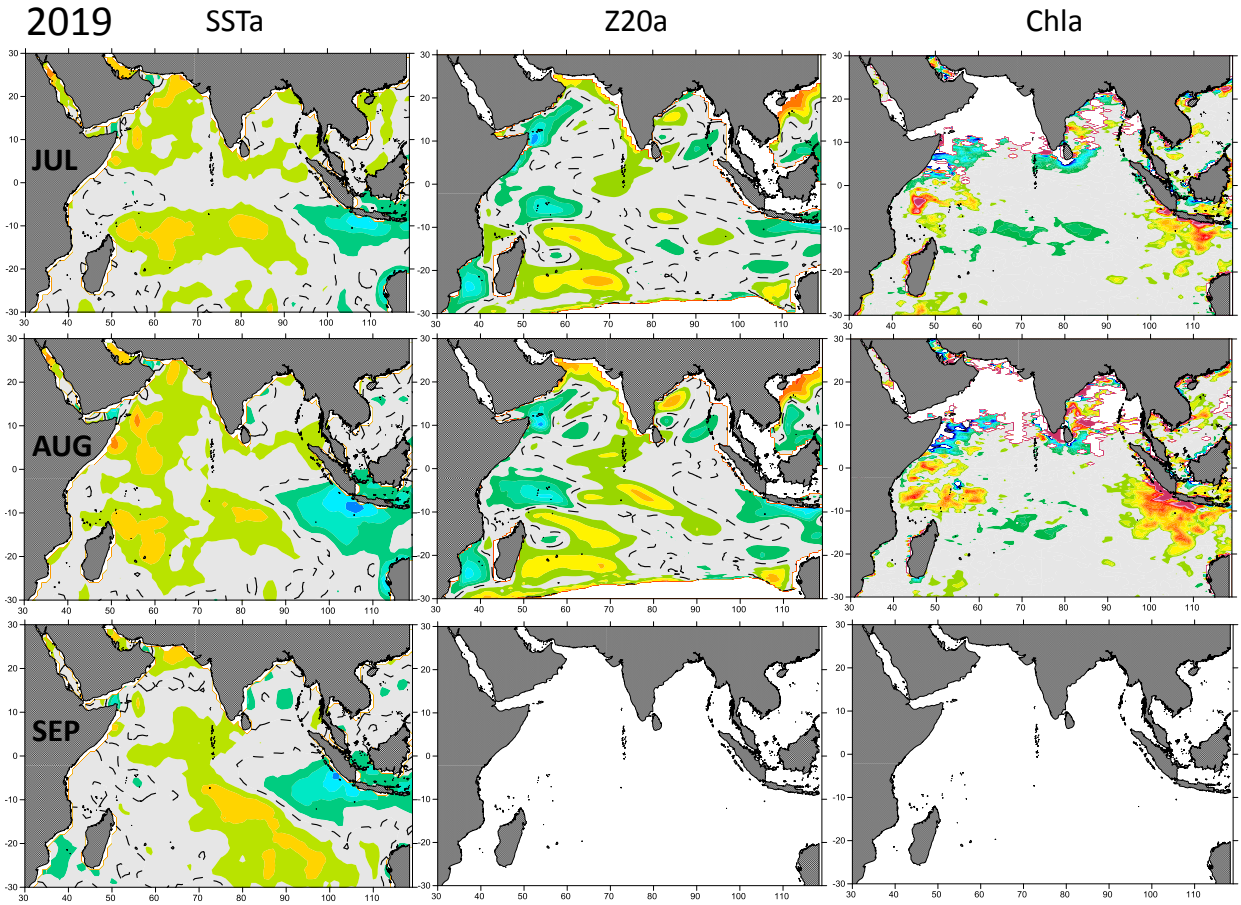

Fig. 6f – Same as above, for the third quarter of 2019

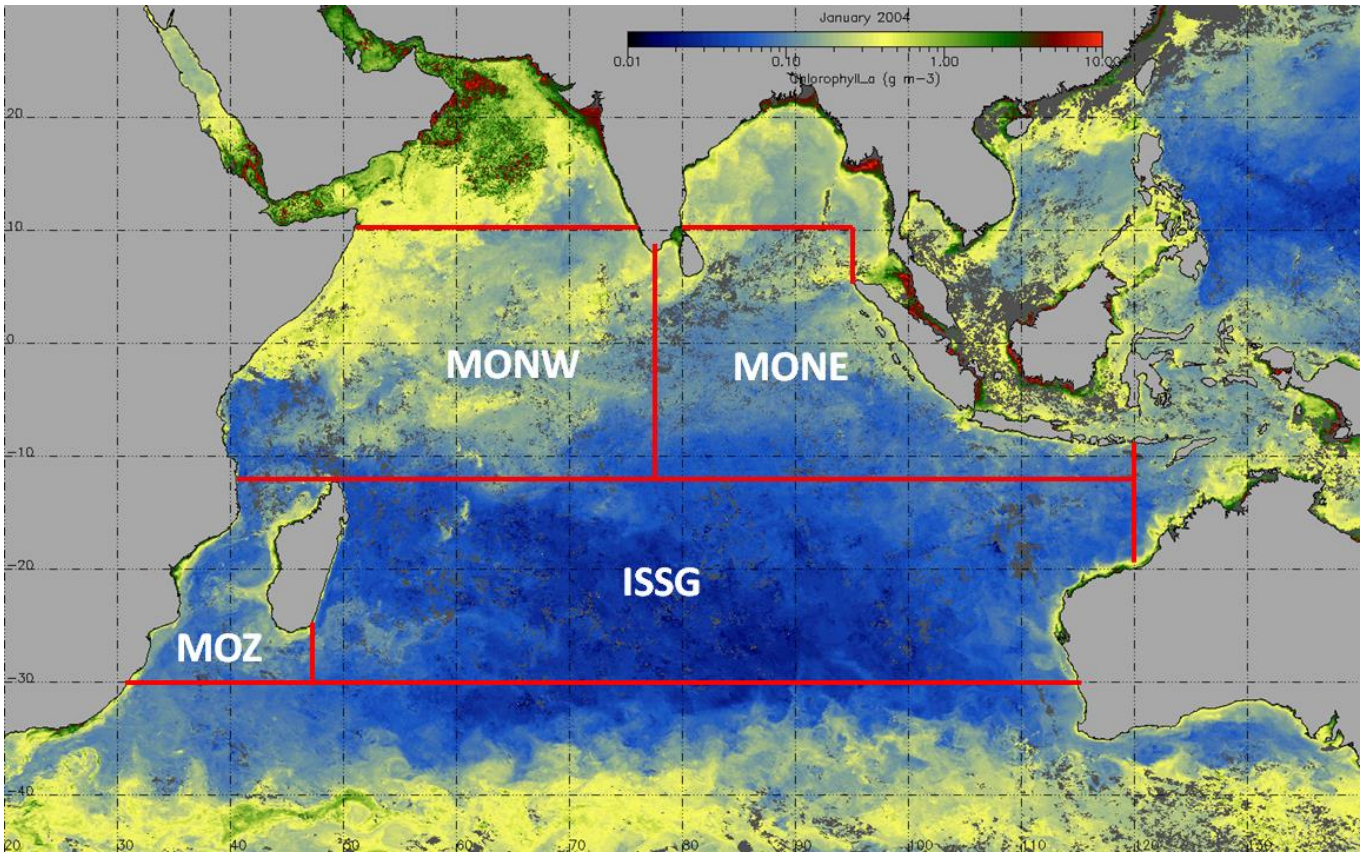

Fig. 7 – Geographical distribution of the four ecoregions studies in this paper. The background image is the chlorophyll concentration measured by MODIS in January 2004.

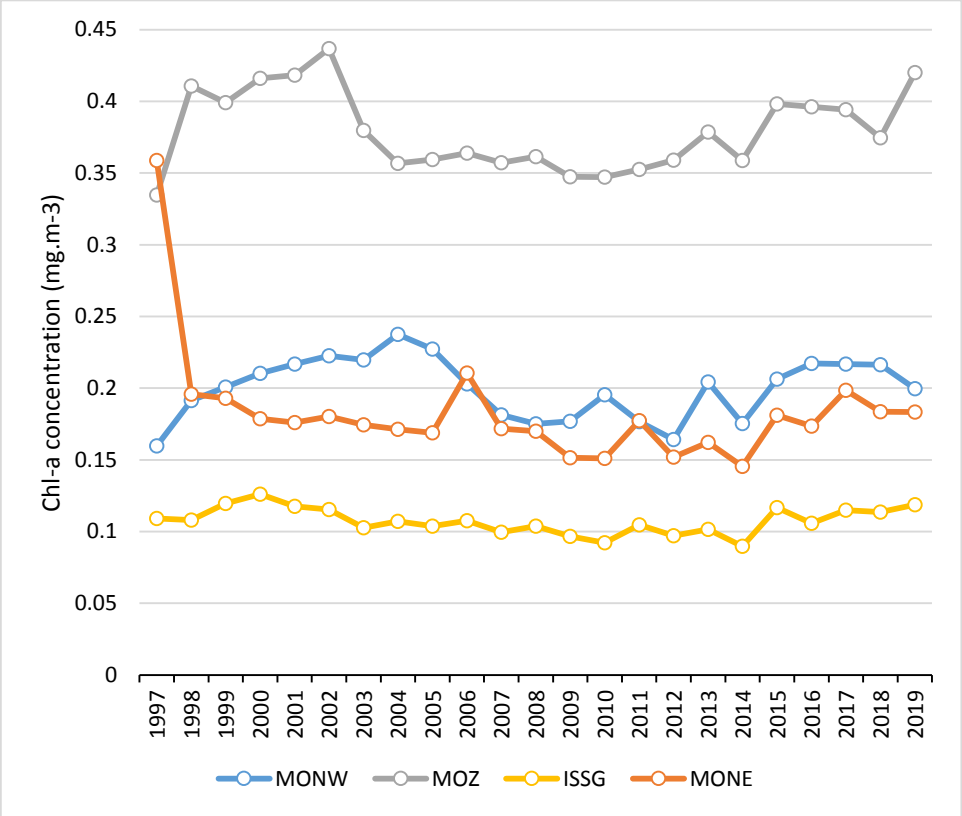

Fig. 8 - Mean annual SSC for each large ecoregion

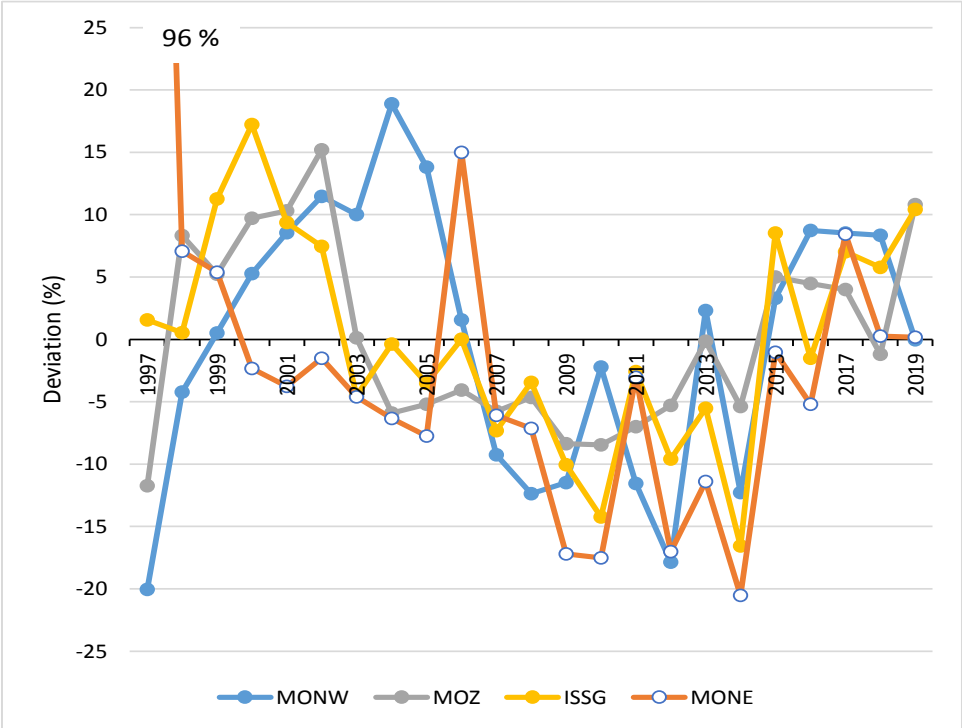

Fig. 9 – Deviation (in %) to the mean multi-annual SSC by large ecoregion

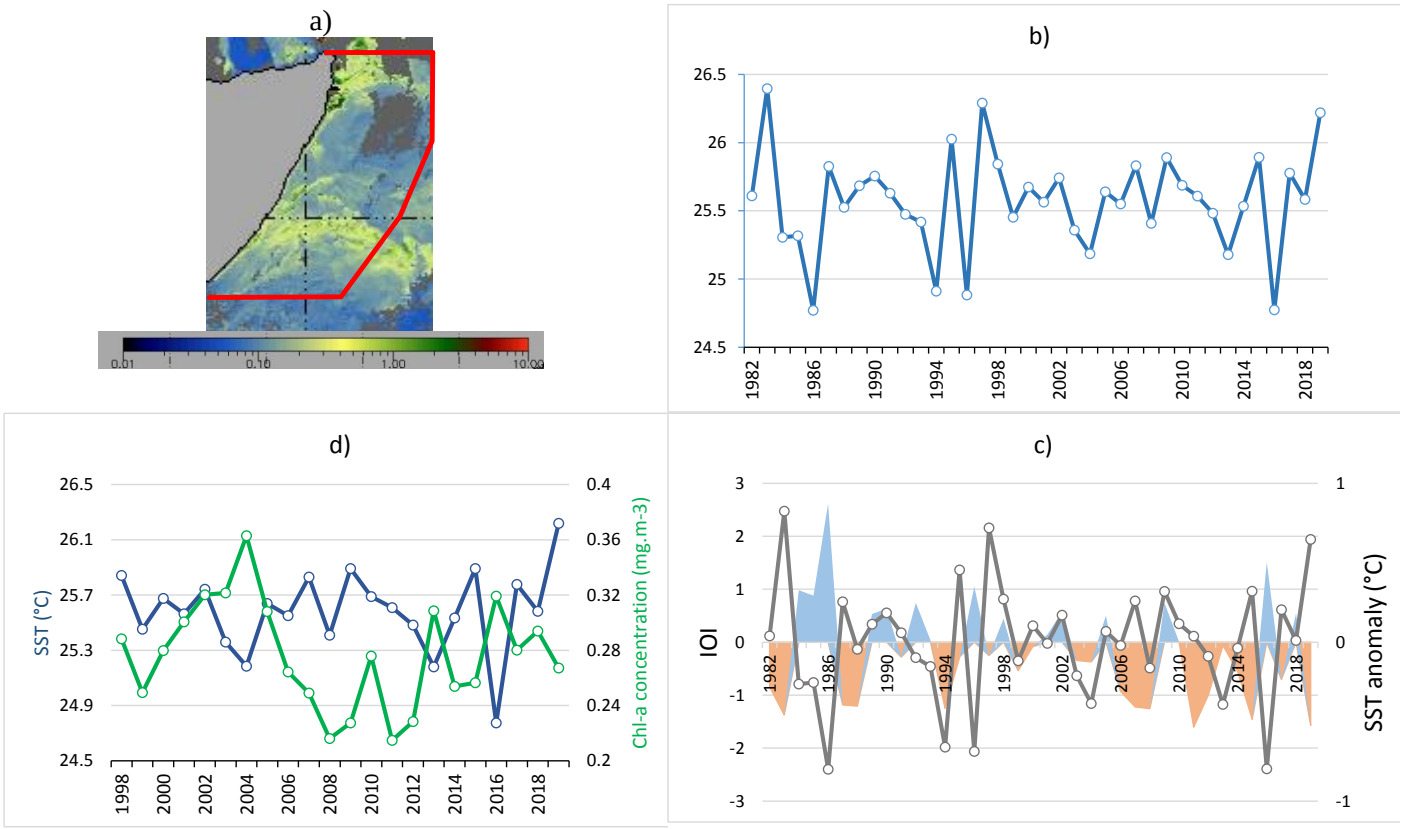

Fig. 10 – Somali upwelling, July to September. a) study area, inside the red line; b) SST, 1892-2019 ; c) SST anomaly (plain line) and IOI (color shaded) from 1982 to 2019; d) SST (study area) and chlorophyll concentration in the MONW ecoregion, 1998-2019.

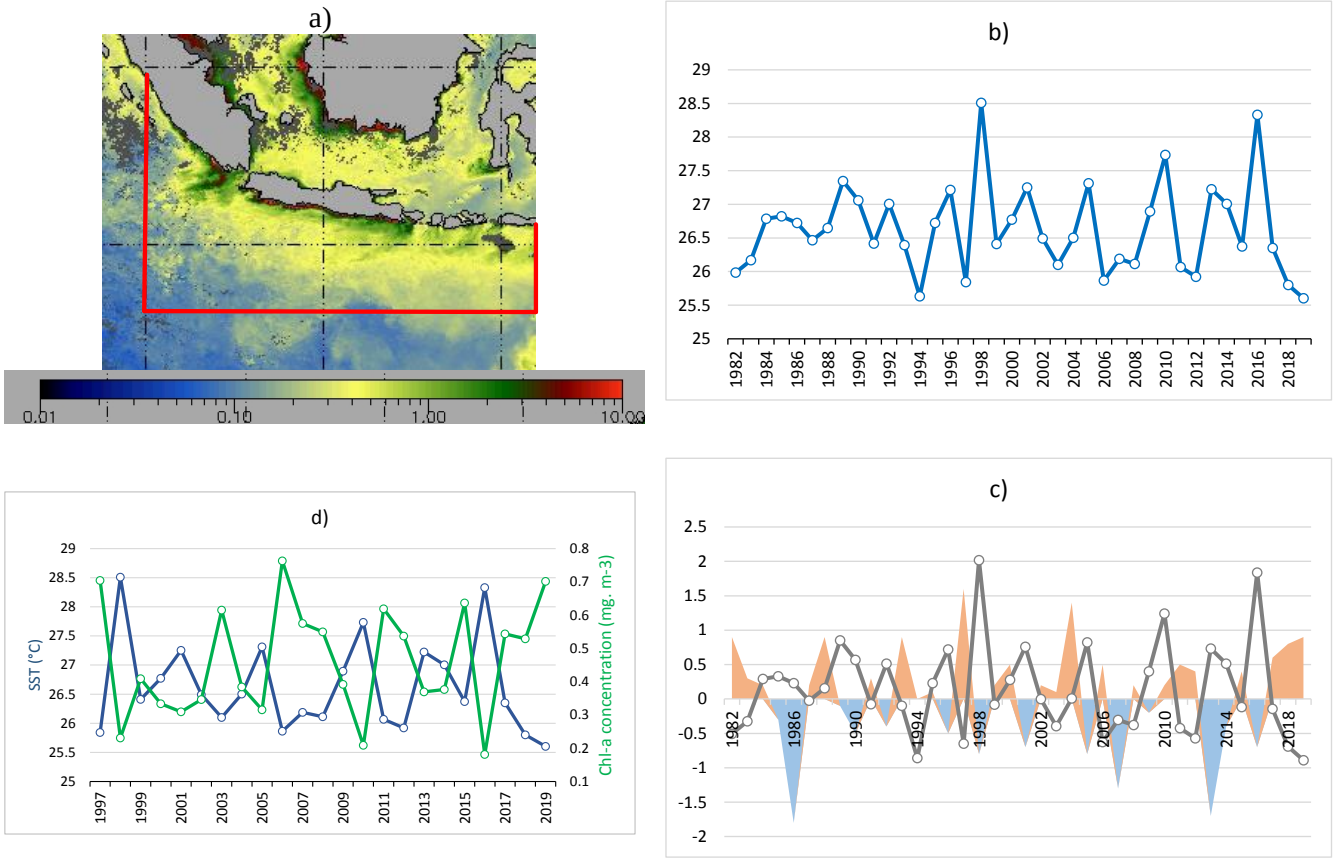

Fig. 11 – Java-Sumatra upwelling, July to September. a) study area, inside the red line; b) SST, 1892-2019 ; c) SST anomaly, in °C (plain line) and Sea Level Pressure anomalies (in hPa) in Darwin (color shaded) from 1982 to 2019; d) SST and Chlorophyll concentration, 1998-2019.